Macromolecules

Article

pubs.acs.org/Macromolecules

Redox-Degradable Biocompatible Hyperbranched Polyglycerols: Synthesis, Copolymerization Kinetics, Degradation, and Biocompatibility

Suhyun Son, Eeseul Shin, and Byeong-Su Kim*

Department of Chemistry and Department of Energy Engineering, Ulsan National Institute of Science and Technology (UNIST), Ulsan 689-798, Korea

Supporting Information

ABSTRACT: Polymers that are biocompatible and degrade in response to stimuli are highly desirable as smart drug-delivery carriers. We report the first novel redox-degradable hyperbranched polyglycerols. A glycerol monomer containing a disulfide bond, i.e., 2-((2-(oxiran-2-ylmethoxy)ethyl)disulfanyl)ethan-1-ol (SSG), was designed and polymerized through anionic ring-opening multibranching polymerization to yield a series of redox-degradable hyperbranched polyglycerols (PSSGs) with controlled molecular weights (2000–11 000 g/mol) and relatively low molecular weight distributions (M_w/M_n < 1.15). In addition, copolymerization with a nondegradable glycerol (G) monomer provided P(G-*co*-SSG) copolymers, which contained an adjustable fraction of degradable moieties within their polyglycerol backbones. The polymerization was characterized using ^{1}H and ^{13}C NMR spectroscopy, GPC, and MALDI-ToF mass spectrometry. The copolymerization process was also evaluated using quantitative *in situ* ^{13}C NMR kinetic measurements in bulk, which revealed that the reaction kinetics of G were faster than those of the SSG monomer, leading to a gradient during the copolymerization process. Furthermore, we explored the redox-responsive degradation of the polymers upon treatment with a reducing agent, which resulted in selective degradation of the polymers in small segments. *In vitro* cytotoxicity studies, such as MTT and CCK-8 assays, revealed the superior biocompatibility of these new polymers even at high concentrations of 500 μg/mL. We anticipate that these novel redox-degradable and highly biocompatible polyglycerols will find applications in a variety of emerging biomedical fields.

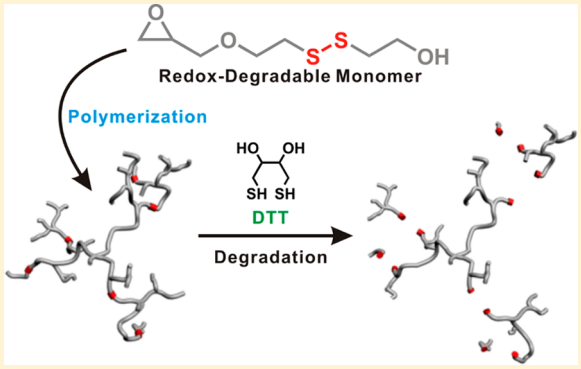

INTRODUCTION

Hyperbranched polyglycerols (PGs) are one of the most popular hyperbranched polymers and possess a globular polymeric structure that comprise a polyether backbone with a large number of hydroxyl groups.[1−3] PGs are typically synthesized via ring-opening multibranching polymerization of glycidol monomers over a broad range of molecular weights with relatively narrow polydispersities.[4,5] Similar to its polyether analogue, poly(ethylene glycol) (PEG), PG exhibits excellent biocompatibility and immunogenicity.[2,6,7] Moreover, owing to their facile synthetic nature and access to various architectures[8−10] as well as the various functional groups that can be installed,[11,12] PGs have attracted significant attention as promising candidates for application in biomedical applications,[13−15] including drug delivery systems,[16−18] polymer therapeutics,[19] proteomics,[20] and human serum albumin substitutes.[21]

The long and controllable *in vivo* circulation half-lives of PGs result in improved therapeutic efficacy;[22] for example, PGs with molecular weights of 100 and 500 kg/mol have circulation half-lives of 32 and 57 h, respectively.[23] However, recent *in vivo* studies have indicated a tendency for relatively high accumulation of higher molecular weight polymers in organs such as the liver; approximately 10% of the injected dose for 500 kg/mol PG accumulated in the liver.[23] Therefore, it remains an important challenge to develop polymers that are biocompatible and degradable under physiological conditions. For this purpose, PGs with acid-degradable moieties were recently introduced. Frey and co-workers developed two types of pH-responsive hyperbranched PGs by incorporating acetal bonds into the monomer or initiator.[24,25] Another approach reported by Kizhakkedathu and co-workers controlled the degradation kinetics of hyperbranched PG introduced by incorporating ketal linkages with different structures into the polymer backbone.[26,27] However, the development of effective polymers that undergo pH-responsive degradation remains incomplete as the polymers could degrade in aqueous solutions even at a neutral pH condition.

Received: November 5, 2014
Revised: January 14, 2015
Published: January 27, 2015

DOI: 10.1021/ma502242v
Macromolecules 2015, 48, 600–609

Scheme 1. Illustration of the Redox-Triggered Degradation of PSSG

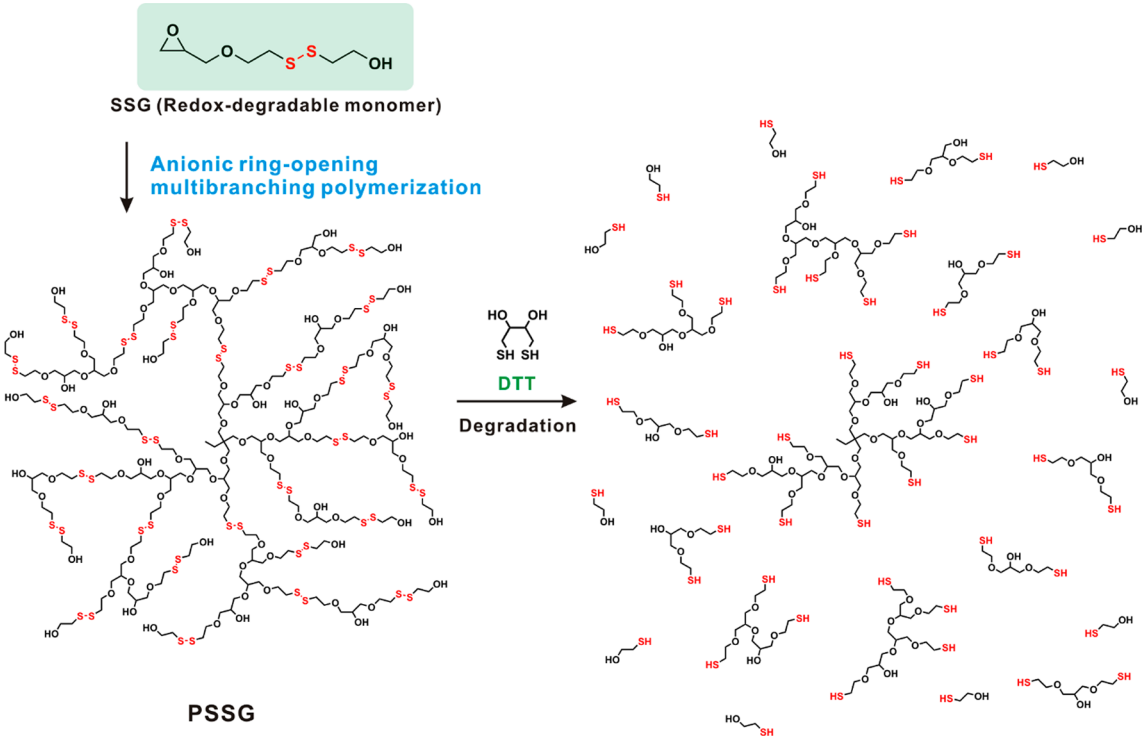

In biological systems, disulfide bonds degrade into their corresponding thiols in response to the reduction potential, which is mainly developed by the higher concentration of glutathione (GSH, 2−10 mM) in cytosol than in the extracellular fluids (<10 μM).[28−30] In contrast, disulfides are stable in the oxidative environments of the cell exterior because of the higher concentration of cystine over cystein and reduced glutathione.[31] Such a large concentration gradient between the intracellular and extracellular environment offer new opportunities for the development of polymers that selectively degrade after uptake into the cells.[32,33] Although there have been reports on the utilization of disulfide bonds for the degradation of PEG- and PG-containing materials,[34−36] many of them are limited to the conjugation linkers between polymers and drugs[37] and cross-linkers for nanogels;[38,39] to the best of our knowledge, there are no reports on the use of disulfide bonds within a PG backbone.

Herein, we present the design and synthesis of novel redox-degradable hyperbranched PGs for the first time (Scheme 1). Specifically, a glycerol monomer containing a disulfide bond, i.e., 2-((2-(oxiran-2-ylmethoxy)ethyl)disulfanyl)ethan-1-ol (SSG), was designed and polymerized through anionic ring-opening multibranching polymerization to yield a series of redox-degradable hyperbranched polyglycerols (PSSGs) with controlled molecular weights (2000−11 000 g/mol) and relatively low molecular weight distributions (M_w/M_n < 1.15). In addition, copolymerization with a nondegradable glycerol (G) monomer provided P(G-*co*-SSG) copolymers containing an adjustable fraction of degradable moieties within the PG backbones. We also investigated the copolymerization kinetics of G and SSG using quantitative *in situ* ^{13}C NMR spectroscopy. In particular, we characterized the degradability of these polymers under redox conditions to elucidate the structures of the polymers after degradation. Finally, we demonstrated the superior biocompatibility of the prepared polymers via cell viability tests.

EXPERIMENTAL SECTION

Materials. All reagents and solvents were purchased from Sigma-Aldrich and Acros and used as received unless otherwise stated. Chloroform-d_1 and deuterium oxide were purchased from Cambridge Isotope Laboratory.

Characterization. ^{1}H NMR spectra were acquired using a VNMRS 600 spectrometer operating at 600 MHz using $CDCl_3$ and D_2O solvents. The number- and weight-averaged molecular weights and molecular-weight distribution were measured using gel permeation chromatography (GPC, Agilent Technologies 1200 series) with a polystyrene (PS) standard and 0.01 M lithium bromide containing dimethylformamide (DMF) as an eluent at 30 °C with a flow rate of 1.00 mL/min. Matrix-assisted laser desorption and ionization time-of-flight mass spectrometry (MALDI-ToF) measurements were carried out on an Ultraflex III MALDI mass spectrometer. The laser system consisted of a pulsed UV laser, an attenuator that allowed fine adjustment of the laser fluence, a lens system to focus the laser beam, and a mirror system to direct the beam into the ion source on the target plate. The standard was a N_2 laser with a 337 nm wavelength (pulse energy of 150 μJ) and 3 ns pulse width for use with matrix components that absorb light of this wavelength (IVB product). 2,5-Dihydroxybenzoic acid (DHB) was used as the matrix. A 10 g/L solution of the polymer in methanol and 10 g/L solution of the matrix solution were prepared separately. The two solutions were then mixed, a 1.0 μL aliquot of the mixture was applied to a target plate, and the solvent was evaporated. Differential scanning calorimetry (DSC) was performed using a DSC Q200 model from TA Instruments in the temperature range from −80 to 100 °C at a heating rate of 10 K/min under nitrogen.

Synthesis of SSG (Monomer). A solution of 2-hydroxyethyl disulfide (13.88 g, 0.09 mol) in *tert*-butanol (150 mL) was slowly added to a solution of potassium *tert*-butoxide (7.41 g, 0.09 mol) in *tert*-butanol (225 mL) with stirring for 15 min at room temperature under argon. After stirring for an additional 15 min, excess epichlorohydrin (54.6 g, 0.6 mol) was added dropwise over 30 min

DOI: 10.1021/ma502242v
Macromolecules 2015, 48, 600−609

using a syringe, and the solution was stirred at room temperature for 15 h. The salt that formed was removed via filtration, and the filtrate was removed using a rotary evaporator to yield a mixture of the product, byproduct (diepoxide), and unreacted diol. The crude product was dissolved in 150 mL of methylene chloride and rinsed with water (30 mL) three times. The organic layer was evaporated using a rotary evaporator and dried in a vacuum oven. The mixture was further purified using silica gel column chromatography with an ethyl acetate/hexane (2:1 v/v) eluent to obtain pure SSG monomer as a pale-yellow viscous liquid (6.2 g, 33%). ^{1}H NMR (600 MHz, $CDCl_3$): δ ppm 3.90 (dd, 2H, J = 12.1, 6.0 Hz), 3.85−3.73 (m, 3H), 3.39 (dd, 1H, J = 11.7, 6.1 Hz), 3.19−3.15 (m, 1H), 2.90 (dt, 4H, J = 22.5, 6.1 Hz), 2.82−2.90 (m, 1H), 2.63 (dd, 1H, J = 5.0, 2.7 Hz) 2.20 (t, 1H, J = 6.3 Hz). ^{13}C NMR (150 MHz, $CDCl_3$): δ ppm 70.91, 68.84, 59.66, 50.19, 43.50, 40.56, and 37.8.

Synthesis of Poly(2-((2-(oxiran-2-ylmethoxy)ethyl)-disulfanyl)ethan-1-ol) (PSSG Homopolymer, Polymer 3). Trimethylolpropane (TMP) (24 mg, 0.1788 mmol) was placed in a two-neck round-bottom flask. Potassium methoxide in methanol (25 wt %, 20 μL, 0.0678 mmol) was diluted with 0.70 mL of methanol and then added to the flask and stirred for 30 min at room temperature under an argon atmosphere. Excess methanol was removed using a rotary evaporator, and the remaining product was dried in a vacuum oven (90 °C, 3 h) to yield a white salt of the initiator. The flask was then purged with argon and heated to 90 °C. The SSG monomer (0.75 g, 3.57 mmol) was added dropwise over 12 h using a syringe pump. After complete addition of the monomer, the reaction was continued for an additional 5 h. After dissolving the PSSG polymer in 1.0 mL of methanol, the homogeneous polymer solution was precipitated into excess diethyl ether and washed twice with diethyl ether. The resulting polymer was dried under vacuum at 90 °C for 1 day. The M_n of polymer **3** was 3709 g/mol, as calculated from the NMR data shown in Figure 2b using the following equation: number of repeating units (n) = 22 (integration value) × 3 (number of protons in TMP (methyl, 3H))/4 (number of protons neighboring the disulfide moiety of SSG (4H)) = 17; M_n = 210.31 (molecular weight of the SSG monomer) × 17 + 134.17 (molecular weight of the TMP initiator) = 3709.44 g/mol.

Synthesis of Poly(glycerol-*co*-2-((2-(oxiran-2-ylmethoxy)-ethyl)disulfanyl)ethan-1-ol) (P(G-*co*-SSG) Copolymer, Polymer 6). TMP (24 mg, 0.1788 mmol) was placed in a two-neck round-bottom flask. Potassium methoxide in methanol (25 wt %, 20 μL, 0.0678 mmol) was diluted with 0.70 mL of methanol and then added to the flask and stirred for 30 min at room temperature under an argon atmosphere. Excess methanol was removed using a rotary evaporator, and the resultant product was dried in a vacuum oven (90 °C, 3 h) to yield a white salt of the initiator. The flask was purged with argon and heated to 90 °C. A mixture of SSG (0.757 g, 3.6 mmol) and glycidol (G) (0.266 g, 3.6 mmol) was added dropwise over 12 h using a syringe pump. After complete addition of the monomer, the reaction was continued for an additional 5 h. The resulting P(G-*co*-SSG) polymer was dissolved in 1.0 mL of methanol; the homogeneous polymer solution was then precipitated into excess diethyl ether, and the precipitate was washed twice using diethyl ether. The resulting polymer was dried under vacuum at 90 °C for 1 day. The M_n of polymer **6** was 4424 g/mol, as calculated from the NMR data shown in Figure 2c using the following equation: number of repeating units (SSG) = 17.47 (integration value) × 3 (number of protons of TMP (methyl, 3H))/4 (number of protons neighboring the disulfide moiety of SSG (4H)) = 13, number of repeating units (G) = [75.52 (integration value) × 3 (number of protons of TMP (methyl, 3H)) − {(13 (number of SSG repeating units) × 9 (number of protons of SSG except those that neighbor the disulfide moiety (9H))) − 6 (number of protons of TMP (ether, 6H))}]/5 (number of protons of the G monomer (5H)) = 21; M_n = 74.08 (molecular weight of the G monomer) × 21 + 210.31 (molecular weight of the SSG monomer) × 13 + 134.17 (molecular weight of TMP) = 4423.88 g/mol.

Polymer Degradation. The degradation of PSSG through disulfide reduction was studied using NMR spectroscopy and GPC as follows: For the NMR analysis, the redox-dependent degradation of the polymers was studied by comparing the chemical shift values before and after treatment with a solution of 2 equiv (against disulfide bond in polymer backbone) of dithiothreitol-d_{10} (DTT-d_{10})-containing D_2O. For the NMR study, approximately 15 mg of the PSSG polymer was dissolved in 0.60 mL of the DTT solution. The reduction of disulfide and degradation of the polymers were monitored by ^{1}H and ^{13}C NMR spectroscopy, respectively. For the GPC analysis, DTT (2 equiv of the disulfide) was added to a solution of P(G-*co*-SSG) in DMF, and the sample was analyzed using GPC-MALLS in DMF containing 10 mM lithium bromide. The molecular weights (i.e, M_n and M_w) and PDI were measured, and the results before and after DTT treatment were compared.

^{13}C NMR Kinetics. To generate the initiator, methoxyethanol (0.5 g, 6.57 mmol) and cesium hydroxide monohydrate (0.378 g, 2.25 mmol) were reacted in a round-bottom flask under an argon atmosphere at 50 °C. The initiator solution (30 μL) was added into the comonomer mixture of G (0.177 g, 2.39 mmol) and SSG (0.504 g, 2.39 mmol) that was placed in a 4.0 mL vial and stirred over an ice bath. The mixture was transferred to a conventional NMR tube under an argon atmosphere and then sealed with a septum over an ice bath. The kinetic measurements using ^{13}C NMR spectroscopy were recorded on a 600 MHz VNMRS system with a 5 mm PFG AutoX DB probe in neat solutions. A standard kinetic ^{13}C NMR experiment required 64 transients that were obtained with a 13.7 μs 90° pulse, spectral width of 1894 Hz, and recycling delay of 10 s for each kinetic run; 70 experiments were performed over a period of 13 h with a flip angle of 45° and inverse gated decoupling.

Cytotoxicity Assay. Human epithelial carcinoma cells (HeLa) and human diploid cells (WI-38) were purchased from the Korean Cell Line Bank (Seoul, Korea). Cytotoxicity assays were performed using the traditional MTT assay. Cells were seeded in 96-well plates at a density of 7 × 10^3 cells per well and incubated for 24 h in 5% CO_2 at 37 °C. HeLa cells were cultured with Dulbecco's Modified Eagle's Medium (DMEM; Life Technologies) with 10% fetal bovine serum (FBS) and 1% penicillin−streptomycin. WI-38 cells were incubated in Roswell Park Memorial Institute (RPMI) 1640 media (Life Technologies) with 10% FBS, 25 mM sodium bicarbonate, and 1% penicillin−streptomycin. After removing the culture medium, the wells were washed with PBS. Each well was then refilled with 90 μL of fresh media and 10 μL of various concentrations of PG_{150}, $P(G_{60}$-*co*-$SSG_{30})$, and $PSSG_{20}$ solutions and incubated for an additional 24 h. For the MTT assays, each well was washed with PBS and then filled with 10 μL of thiazolyl blue tetrazolium bromide (MTT; Sigma-Aldrich) stock solution (5 mg/mL) and 90 μL of fresh media. After incubation for 4 h, 100 μL of DMSO was added to the polymer solution to solubilize the MTT-formazan product, and the plates were gently agitated for 15 min at room temperature. The absorbance of the solution was recorded at a wavelength of 540 nm using 620 nm as the reference. For the CCK-8 assays, each well was washed with PBS and then filled with 10 μL of water-soluble tetrazolium salt (CCK-8; Dojindo Molecular Technologies) and 90 μL of fresh media. After incubation for 4 h, the plates were gently agitated for 15 min at room temperature, and the absorbance of the solution was recorded at a wavelength of 450 nm.

RESULTS AND DISCUSSION

A. Polymer Synthesis and Characterization. To produce redox-degradable and multifunctional hyperbranched polyglycerol, we first designed and synthesized a redox-labile AB_2-type monomer, i.e., SSG (Figure 1a). In the SSG monomer, the disulfide bond is a redox-labile linkage, and the hydroxyl group plays a role as a branching reaction site. The disulfide linkage was introduced between epoxide and hydroxyl groups using 2-hydroxyethyl disulfide, as shown in Figure 1a. The successful synthesis of the monomer SSG was confirmed via characterization using ^{1}H and ^{13}C NMR spectroscopy (Figure 2a, Figure S1 and Figure S2 in the Supporting Information).

DOI: 10.1021/ma502242v
Macromolecules 2015, 48, 600−609

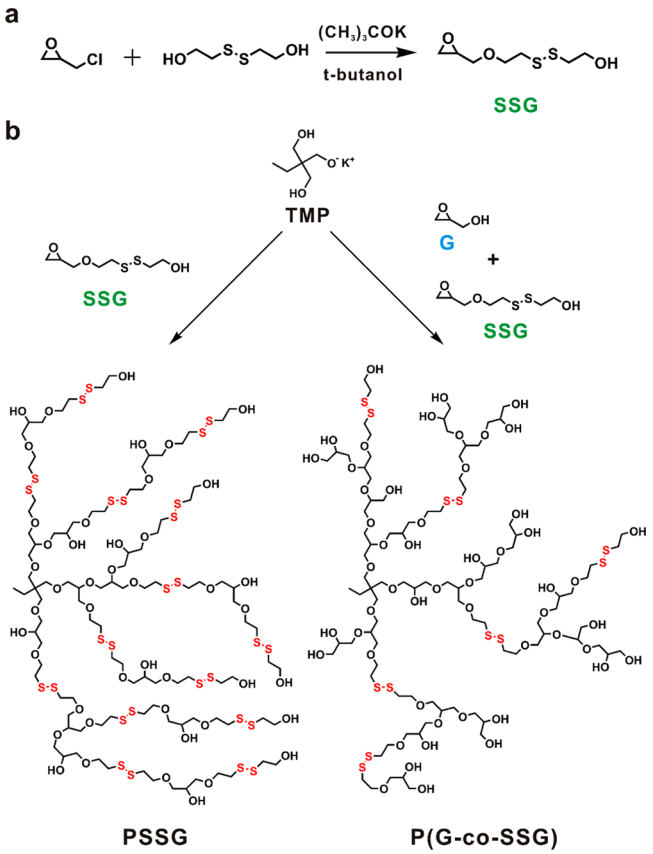

Figure 1. Synthetic pathways for the preparation of (a) redox-active disulfide monomer (SSG) and (b) polymers from pure SSG monomers to yield the PSSG homopolymer and from SSG and glycerol monomers (G) to generate the P(G-*co*-SSG) copolymer.

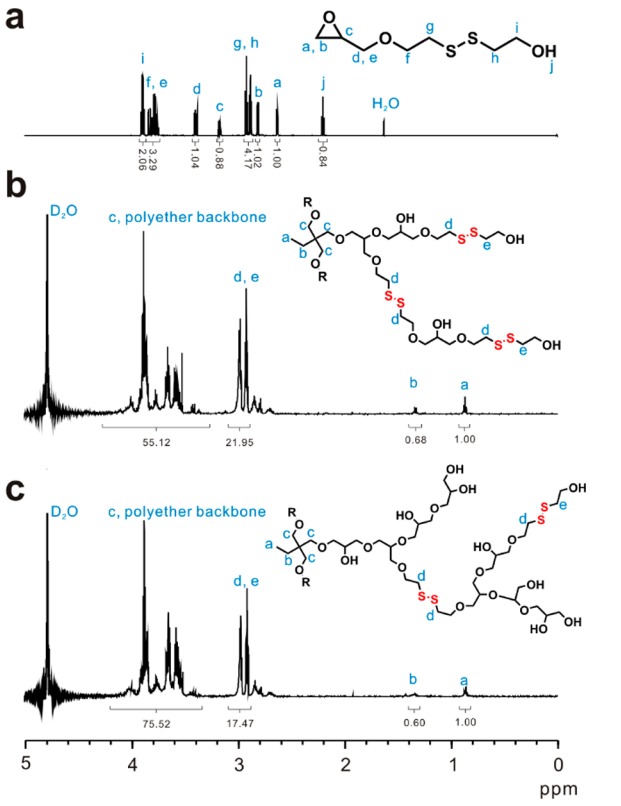

Figure 2. ^{1}H NMR spectra of (a) SSG monomer in $CDCl_3$, (b) PSSG homopolymer (polymer **3**) in D_2O, and (c) P(G-*co*-SSG) copolymer (polymer **6**) in D_2O.

After successful synthesis of the SSG monomer, we studied their anionic ring-opening multibranching polymerization using a potassium alkoxide initiator that was formed via the reaction of TMP and potassium methoxide solution (Figure 1). As demonstrated in previous works, we employed a slow monomer addition method to synthesize the polymers in a controlled manner.[10,16,17] The molecular weights of the polymers were controlled via the monomer-to-initiator ratio and characterized using GPC and ^{1}H NMR spectroscopy. In all cases, controlled molecular weights (PSSG homopolymer: 2200−10 600 g/mol; P(G-*co*-SSG) copolymer: 5000−24 000 g/mol) and narrow molecular weight distributions (M_w/M_n: <1.15 for the homopolymer, <1.38 for the copolymer) were obtained considering the branched structures of the products and the PS standard used (Table 1). Interestingly, we observed that the SSG monomer converted completely for the homopolymer (90−100%); however, the addition of glycidol as a comonomer slightly decreased the SSG conversion (60−85%). This result suggests different reactivity of the two monomers, which will be described in detail in the following discussion. In addition, by varying the feed composition of SSG (25−75 mol %) in the polymerization of the P(G-*co*-SSG) copolymers, we achieved various compositions of P(G-*co*-SSG) with incorporation ratios of SSG ranging from 28 to 55 mol %.

All synthesized PSSG and P(G-*co*-SSG) polymers were soluble in water and organic polar solvents such as methanol, DMSO, and DMF. As shown in Figure 2b, the ^{1}H NMR spectra of the homopolymer (polymer **3**) clearly showed the characteristic peaks corresponding to the protons on the carbon atoms adjacent to the disulfide moiety (peaks d and e at 2.9−3.1 ppm), the methyl and methylene groups of TMP (peaks a and b at 0.8 and 1.3 ppm, respectively), and polyether backbone (polyether backbone of PSSG and peak c at 3.4−4.2 ppm). By determining the ratio of the integrals of the peaks for the initiator (0.8 ppm) to the protons on the carbon atoms that neighbor the disulfide moiety (2.9−3.1 ppm), we calculated the M_n values (see the Experimental Section and Figure S3 for detailed calculations). Overall, we found good agreement between the target molecular weight and the data obtained from NMR spectroscopy.

Moreover, the ^{1}H NMR spectrum of the copolymer (polymer **6**) shows similar chemical shifts as that of the homopolymer (Figure 2c). However, polyether backbone signal (3.4−4.2 ppm) was more intense for the copolymer than for the homopolymer, which was attributed to the additional polyether backbone present in PG. The incorporation ratio of SSG and the molecular weight were calculated by integrating the peaks of the protons on the carbon atoms adjacent to the disulfide moiety at 2.9−3.1 ppm (SSG) and on the polyether backbone at 3.4−4.2 ppm against the signal of the initiator at 0.8 ppm (see the Experimental Section and Figure S4 for detailed calculations). It is of note that the peaks observed at 2.8−2.9 ppm are considered as methylene protons of CH_2−S−CH_2 (thioether) and/or CH_2−SH (thiol). These products could be originated from the side reactions of sensitive disulfide bond with a good nucleophilic alkoxide anion under the polymerization condition. Although the nondegradable thioether moiety could affect the degradation nature of the polymers, the effect is negligible as the fraction is relatively small (less than 16%), and it is still connected through the

DOI: 10.1021/ma502242v
Macromolecules 2015, 48, 600−609

Table 1. Characterization Data for All Polymers Synthesized in This Study

no.	polymer composition (target)	polymer composition (NMR)[a]	M_n (target)	% SSG (target)	M_n (NMR)[a]	% SSG (NMR)[a]	M_n (GPC)[b]	M_w/M_n (GPC)[b]
1	PG_{150}	PG_{139}	11200	0	10400	0	14300	1.50
2	$PSSG_{10}$	$PSSG_{9}$	2240	100	2030	100	3780	1.10
3	$PSSG_{20}$	$PSSG_{17}$	4340	100	3710	100	3600	1.12
4	$PSSG_{50}$	$PSSG_{53}$	10650	100	11280	100	5010	1.15
5	$P(G_{10}$-*co*-$SSG_{20})$	$P(G_{10}$-*co*-$SSG_{12})$	5080	66.67	3530	54.54	4620	1.23
6	$P(G_{20}$-*co*-$SSG_{20})$	$P(G_{21}$-*co*-$SSG_{13})$	5820	50.00	4420	38.23	5000	1.25
7	$P(G_{60}$-*co*-$SSG_{30})$	$P(G_{46}$-*co*-$SSG_{18})$	10890	33.33	7460	28.12	5370	1.38
8	$P(G_{165}$-*co*-$SSG_{55})$	$P\{G_{114}$-*co*-$SSG_{48}\}$	23920	25.00	18670	29.63	15800	1.28

[a]Determined via ^{1}H NMR spectroscopy. [b]Measured using GPC-RI in DMF with a polystyrene standard.

degradable disulfide linkages along the backbone of the polymers. In addition, we confirmed the branched structure of the PSSG polymers via detailed analysis of the ^{1}H and inverse-gated ^{13}C NMR spectra (see Supporting Information Figures S6–S9 and description for details).

The GPC results showed a monomodal distribution and controlled molecular weight values (Table 1). However, there was a discrepancy between the molecular weights determined by NMR spectroscopy and GPC; this was explained by the branched architecture and presence of multiple hydroxyl functional groups because these globular hyperbranched structures do not contribute to the overall hydrodynamic radius of the polymers.[40] Calibration of GPC with PS could be another source of deviation.

The presence of the TMP initiator and functional monomer segments in PSSG and P(G-*co*-SSG) polymers was clearly confirmed via MALDI-ToF spectroscopy (Figure 3). As shown in Figure 3a, two distribution modes were observed because of the coordination of different ions, such as H^+ and K^+. For example, the main molecular weight peak at 1224.82 g/mol corresponded to the molecular weight of PSSG with K^+ as a counterion (TMP(134.17) + SSG(210.31) × 5 + K^+(39.1)), and the peak at 1186.72 g/mol corresponded to the molecular weight of PSSG with H^+ as a counterion (TMP(134.17) + SSG(210.31) × 5 + H^+(1)). In addition, the spacing between the signals (210.31 g/mol) matched well with the functional SSG unit incorporated into PSSG, which confirmed the presence of the SSG monomer.

Unlike the result of PSSG homopolymer, the MALDI-ToF results for the P(G-*co*-SSG) copolymer revealed the presence of complex distribution modes. As shown in Figure 3b, the presence of the TMP-initiated copolymer of G and SSG is clearly proved. In particular, the peaks that corresponded to the copolymer with various combinations of G and SSG were isolated from the complex mass spectrum (inset in Figure 3b); for example, the mass peak at 2670.63 g/mol corresponded to the copolymer with TMP as an initiator, 11 units of G, 8 units of SSG, and K^+ as a counterion (TMP(134.17) + G(74.08) × 11 + SSG(210.31) × 8 + K^+(39.1)). It should be highlighted that the spacing of the signals corresponded to the mass of a linear combination of the respective monomers in the copolymer (G: 74.08 g/mol; SSG: 210.31 g/mol) in varying degrees, which unambiguously demonstrated the successful copolymerization of P(G-*co*-SSG).

Independent of the MALDI-ToF experiment, we further verified the structures and thermal properties of copolymers by DSC measurement. According to the DSC measurements presented in Figure 4, we confirmed that the glass transition temperature, T_g, of copolymer $P(G_{167}$-*co*-$SSG_{56})$ (−34 °C) was

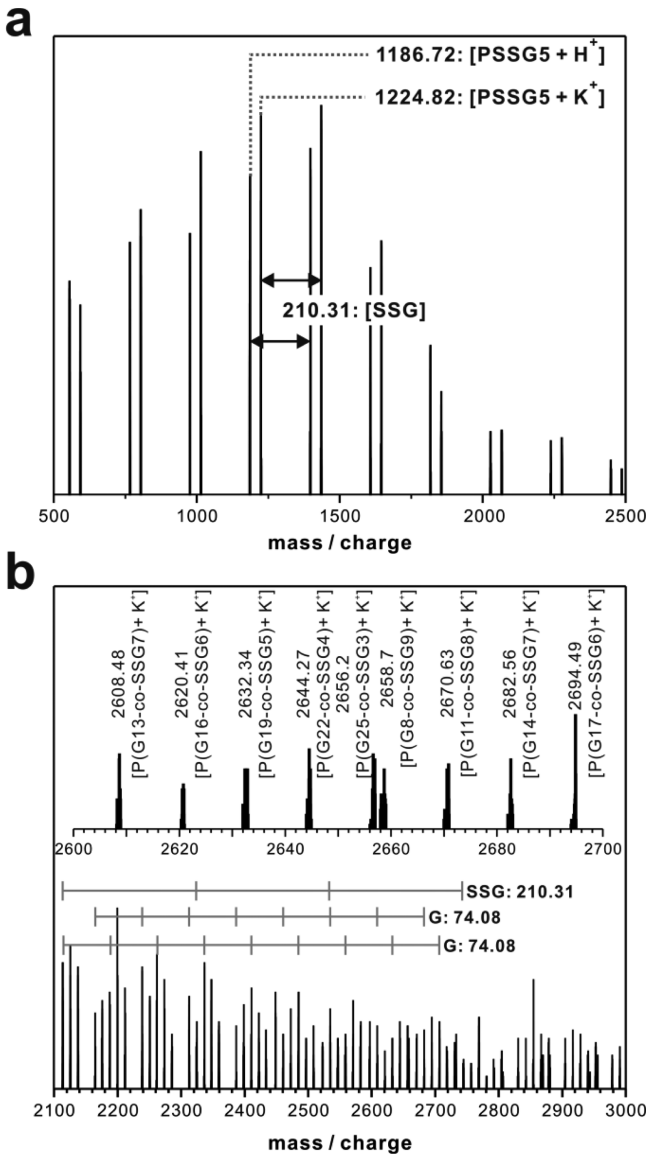

Figure 3. MALDI-ToF spectra of the (a) $PSSG_{10}$ homopolymer (polymer **2**) and (b) $P(G_{10}$-*co*-$SSG_{20})$ copolymer (polymer **5**) using DHB as a matrix. The inset in (b) shows the detailed molar mass and assignments of the copolymer in the range of 2600–2700 g/mol. The spacing of the signals corresponds to the mass of a linear combination of the respective monomers in the homopolymer and copolymer (G: 74.08 g/mol; SSG: 210.31 g/mol).

observed between that of respective PG_{150} (−25 °C) and $PSSG_{50}$ (−48 °C) homopolymers. This result suggests the

DOI: 10.1021/ma502242v
Macromolecules 2015, 48, 600–609

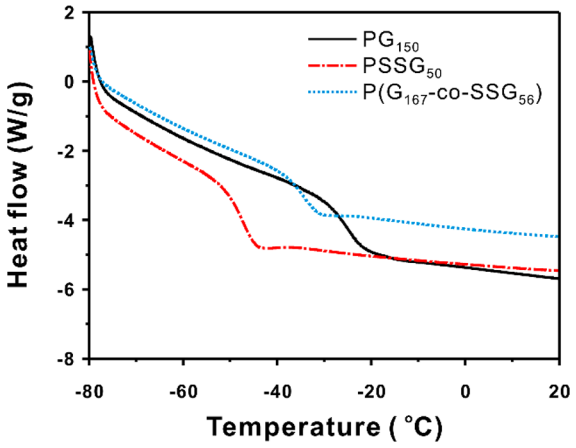

Figure 4. DSC graphs for PG_{150} (black), $PSSG_{50}$ (red), and $P(G_{167}$-*co*-$SSG_{56})$ (blue).

successful synthesis of copolymer without phase separation. In contrast to a single T_g observed for the copolymer, two different T_gs were found in a simple blend of two homopolymers (−30 and −44 °C, respectively) (Supporting Information Figure S10).

B. *In Situ* Copolymerization Kinetics. As we developed the novel SSG monomer, it was essential to investigate its copolymerization behavior with other monomers for analysis of the comonomer distribution during the copolymerization. To observe the kinetics of the epoxide monomer, online ^{1}H NMR spectroscopy is generally employed as it is readily accessible with an interval as short as a few seconds between two spectra and is a quantitative method to monitor the consumption of comonomers.[12,40,41] However, the ^{1}H NMR signals of both monomers and the polymer overlapped in our case, which limited the monitoring of monomer consumption. Therefore, we employed quantitative and *in situ* monitoring of both monomers for bulk copolymerization based on ^{13}C NMR spectroscopy according to a recent development reported by Frey and co-workers.[42] Specifically, copolymerization of G and SSG was conducted without any solvent at 50 °C in a conventional NMR tube. During bulk polymerization, a quantitative ^{13}C NMR spectrum could be obtained within a few minutes because of the sufficient natural abundance of ^{13}C isotope. With this method, we could observe the microstructure of the growing polymer at any time during the reaction.

Figure 5 shows a typical series of ^{13}C NMR spectra collected during the copolymerization of G and SSG that demonstrate the consumption of both monomers (G highlighted in blue and SSG in red) with the concomitant appearance of the polyether backbone of the polymers at 70−78 ppm. To assess the monomer consumption, the resonances for the representative carbon in the methine group for both epoxide monomers (at 55 and 53 ppm for G and SSG, respectively) were compared during the progress of the reaction. As shown in Figure 5, the time required for full monomer consumption of G was shorter than that of SSG: The signals for the G and SSG monomers could not be detected after 165 and 440 min, respectively, indicating the different reactivity of each monomer. This difference could be attributed to the structure of the disulfide spacer within SSG, which would hinder the approach of another SSG monomer, thus reducing the reactivity of SSG during polymerization, as has been similarly observed in other studies.[27] Meanwhile, we chose 50 °C for the polymerization temperature in the kinetics study to prevent any potential explosion in the NMR tube caused by the low flash point of the glycidol monomer (66 °C). We believe that the polymerization temperature could affect the overall reaction rate; however, the relative reactivity of each monomer would not alter at different temperatures.[12,40]

The monomer conversion ratio of both G and SSG monomers was plotted against the total conversion ratio during copolymerization, as shown in Figure 6. It should be noted that the monomer conversions in the first ^{13}C NMR spectra were set to 0%, and the conversion ratio was calculated from the integration values of methine group of each monomer against the signal of the two carbon atoms adjacent to the disulfide moiety, which remained constant during polymerization. As shown clearly in Figure 6, the molar ratio of SSG units in the polymer chain was considerably lower than the monomer feed at the initial stage and increased rapidly upon consumption of the G monomer near the final stages of the reaction; for instance, at a total conversion of 51%, the conversions of G and SSG were 80 and 22%, respectively (i.e., G is 3.6 times more reactive than SSG). Thus, there is a gradient of monomer incorporation during copolymerization of P(G-*co*-SSG). Nonetheless, unlike the one-pot reaction in bulk during NMR measurements, we employed a slow monomer addition method to synthesize the copolymers. Thus, we predicted that the difference in the reactivity of the two monomers would be

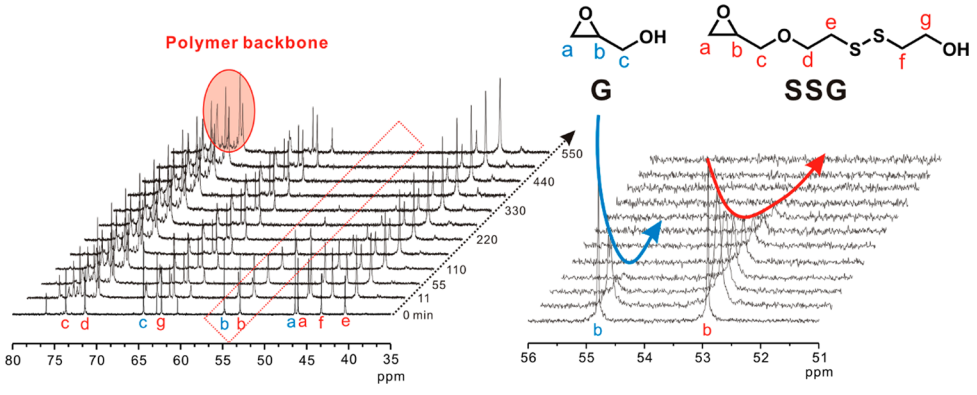

Figure 5. ^{13}C NMR spectra of the *in situ* copolymerization kinetics of G and SSG (initial monomer ratio of 1:1). (left) Overlay of the spectra collected within a designated time period. (right) Zoom-in spectra, showing the signals for the methine carbons of the epoxide at 53 and 55 ppm, which correspond to the G and SSG monomers, respectively (no solvent, 150 MHz, 323 K).

DOI: 10.1021/ma502242v
Macromolecules 2015, 48, 600−609

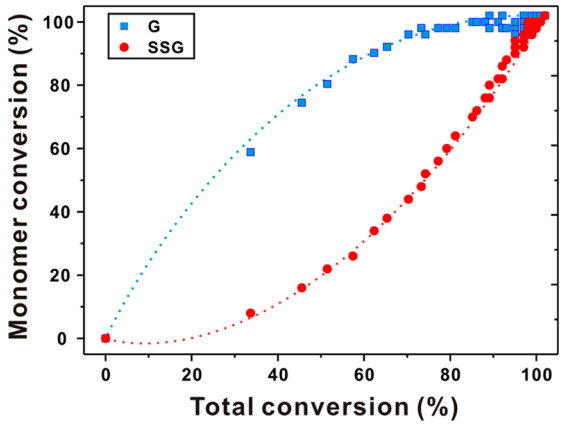

Figure 6. Monomer conversion percentage versus total conversion for copolymerization of G (blue square) and SSG (red circle) (initial monomer ratio of 1:1) determined from quantitative ^{13}C NMR kinetics in bulk at 50 °C.

suppressed to yield more uniform distribution of both monomers.

C. Degradation Study. The presence of disulfide groups in the monomer and polymer chains makes them degradable under reductive conditions. DTT was employed as a reducing agent for the following reasons: It has a high disulfide reduction efficiency because of its conformational tendency for the formation of a stable six-membered ring containing an internal disulfide bond, and it is soluble in various organic solvents that can dissolve the PG-based polymer. To study the DTT-induced degradation of PSSG (Figure 7a), we initially observed the reduction of PSSG by dissolving it in 2 equiv (against disulfide bond in polymer backbone) of a DTT-d_{10}-containing D_2O solution and compared the ^1H and ^{13}C NMR spectra before and after DTT treatment. As shown in the ^1H and ^{13}C NMR results, the signals corresponding to the protons and carbon atoms that neighbor the disulfide moiety disappeared with the concomitant appearance of thiol-neighboring proton and carbon signals upon DTT treatment (Figure 7b). In addition, we confirmed the rapid cleavage of the disulfide bond of polymer chain in a DTT-containing aqueous solution within 10 min; this was attributed to the high solubility of PSSG and DTT in water, which facilitated the access of DTT to the polymer chains.

We have further investigated the degradation products of the copolymer by GPC analysis. Figure 8 shows how the molecular weight of the P(G_{165}-*co*-SSG_{55}) chain changes after DTT-induced degradation in DMF for 1 h. In this study, we employed high molecular weight copolymer of P(G_{165}-*co*-SSG_{55}) for better observation of molecular weight changes upon degradation. As presented in Figure 8a, the molecular weight peak at 18 000 g/mol shifted to the left, indicating the successful degradation of P(G_{165}-*co*-SSG_{55}) into small polymer fragments represented by three peaks centered at 2600, 4600, and 12 900 g/mol, which correspond to small, large, and large core segment in Figure 8b. It is also interesting to note that three respective peaks had different intensities. Considering the higher reactivity of the nondegradable G monomer over the redox-degradable SSG monomer, the inner core block of the copolymer would be comprised more fraction of the non-degradable plain G, while the outer periphery of the copolymer contained would consist of more degradable SSG. This gradient in the distribution of monomers within the hyperbranched

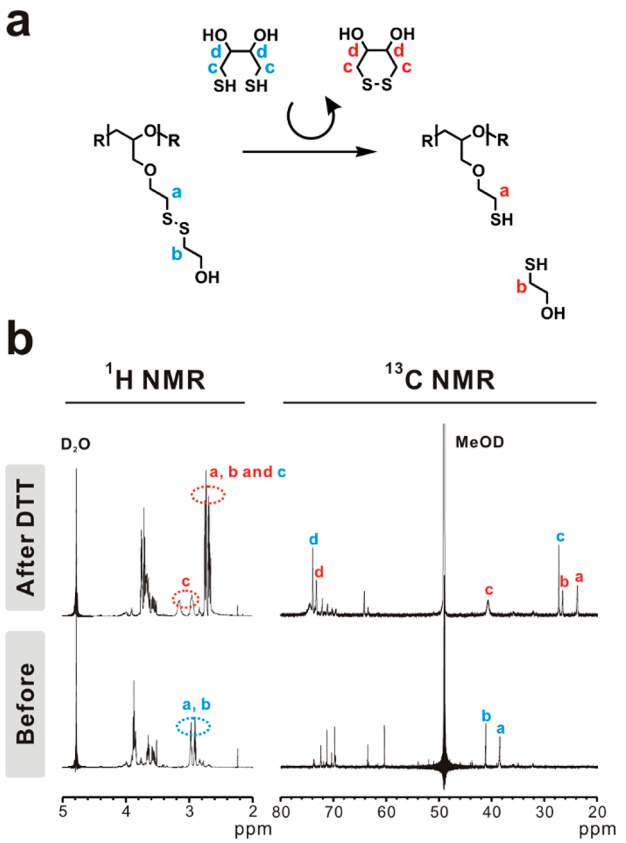

Figure 7. (a) Illustration of degradation of the PSSG chain upon DTT treatment and (b) corresponding changes in the ^1H and ^{13}C NMR spectra of the PSSG homopolymer (polymer **3**) after DTT treatment (10 min).

copolymer of P(G_{165}-*co*-SSG_{55}) resulted in the greater intensity of the lower molecular weight fraction than that of the higher molecular weight fraction (Figure 8b). Along with the experiment of copolymer P(G_{165}-*co*-SSG_{55}), we explored the degradation of homopolymer $PSSG_{50}$ by GPC. In clear contrast to copolymer, homopolymer is degraded into much smaller segment due to absence of nondegradable PG backbone (Supporting Information Figure S11). We also proposed possible mechanistic insights for the degradation of polymers from the differences that were evident during the polymerizations (Figure 8c). Specifically, the incoming monomer resulted in growth of polymer chains via a reaction with either the secondary or primary hydroxyl groups, which are represented as blue and green, respectively. If a monomer reacted with the secondary hydroxyl group, the generated polymer chain would remain even after DTT treatment. In contrast, if the monomer reacted with the primary hydroxyl group, the new polymer chains could be cleaved from the parent polymer chain. Accordingly, the degradation products were divided into small and large segments; the molecular weights of the large segments were almost twice those of the small segments. The presence of the large core segment (large segment with an initiator) was attributed to the TMP initiator bearing three hydroxyl groups. In theory, the TMP initiator could have three large segments, which would result in a large core segment with a molecular weight that was 3 times that of a large segment. In short, the degradation products were divided into three structures depending on the initiator and the two different reaction sites of the monomer.

DOI: 10.1021/ma502242v
Macromolecules 2015, 48, 600−609

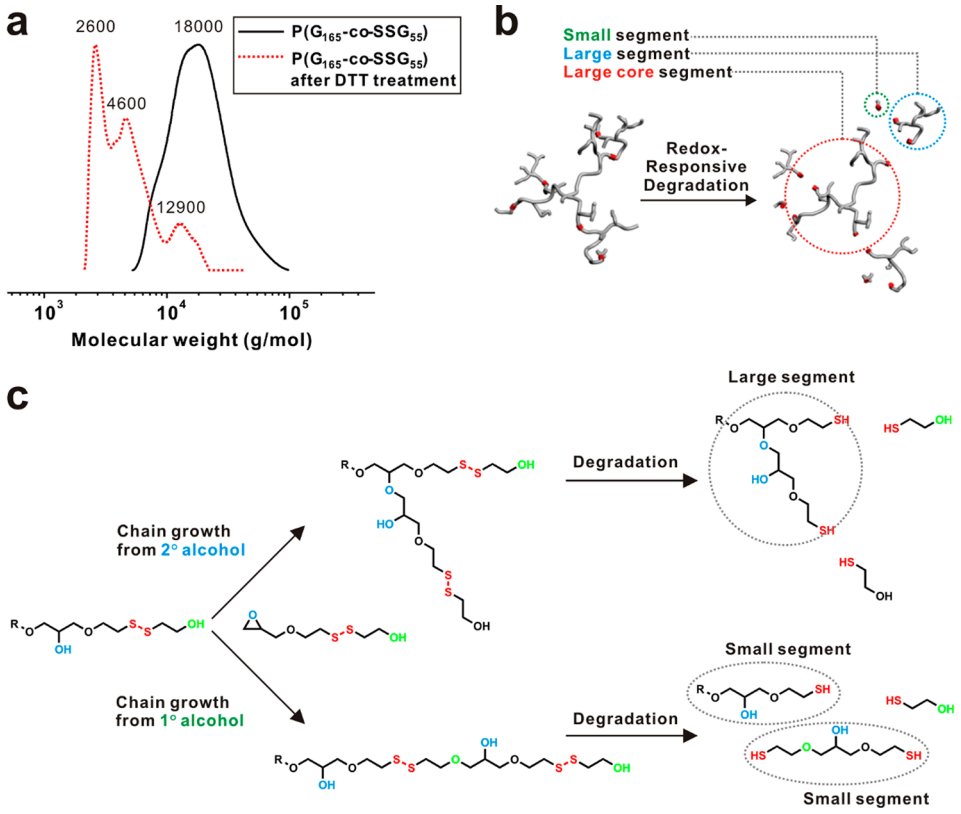

Figure 8. (a) GPC traces of P(G_{165}-*co*-SSG_{55}) (polymer **8**) before (black curve) and after (red curve) DTT treatment. The number on the trace represents the corresponding molecular weight of the peak. (b) Illustration of the degradation products and (c) possible mechanism for the origin of the three peaks in the GPC trace after DTT treatment. The direction of the incoming monomer into the two different hydroxyl groups determines the structures of the degradation products.

D. Biocompatibility Assay. We evaluated the cytotoxicity of PG_{150}, P(G_{60}-*co*-SSG_{30}), and $PSSG_{20}$ to investigate their potential as drug delivery carriers. Each polymer was treated with WI-38 (human diploid cells) and HeLa (human epithelial carcinoma cells) cell lines as models of normal and cancer cells, respectively. The cytotoxicity of each sample was examined using MTT and CCK-8 assays, which are commonly used for *in vitro* cytotoxicity testing of polymers and nanomaterials. The MTT assay is based on mitochondrial dehydrogenase activity, whereas the CCK-8 assay uses an electron mediator, i.e., 1-methoxyphenazinium methylsulfate (1-methoxy PMS), to detect the activity of dehydrogenase, NAD(H), and NADP(H) in the cell. Therefore, the CCK-8 assay is more sensitive than the MTT assay as it reflects the overall cell viability while the MTT assay shows mitochondrial activity.[43] As shown in Figure 9, the cell viability of each cell line treated with various concentrations of polymer solution was greater than 90% up to a concentration of 100 μg/mL in both assays. Although pure PG displayed superior cell viability at all concentration ranges tested as demonstrated in other report,[6] pure $PSSG_{20}$ exhibited relatively low cell viability as compared to the other two samples at a high concentration of 1000 μg/mL; this was due to degradation of the disulfide bond under intracellular redox conditions, which affected the intracellular redox mechanism resulting in moderate cytotoxicity. In general, the P(G_{60}-*co*-SSG_{30}) copolymer with 30 mol % disulfide linkages exhibited a higher cell viability than homopolymer $PSSG_{20}$ at 1000 μg/mL. Taken together, these results corroborated that the number of degradable linkages influenced the overall cell viability. It should be also noted that the content of the degradable linkages in P(G_{60}-*co*-SSG_{30}) is still significantly higher than that of previously reported degradable polymers which contains degradable linkages between 6 and 15 mol %.[26] Considering that the desired concentration for biological application of these polymers is typically lower than 1000 μg/mL, both the homopolymer and copolymer with the novel redox-degradable SSG moieties would have minimal adverse effects on the mitochondrial activity and cell viability.

■ CONCLUSION

In summary, we reported the design and synthesis of novel redox-degradable hyperbranched polyglycerols (PSSGs) from a disulfide-bearing glycerol monomer (SSG). A series of well-defined PSSG homopolymers and P(G-*co*-SSG) copolymers were successfully synthesized via anionic ring-opening multi-branching polymerization of SSG and G, resulting in controlled molecular weights and molecular weight distributions. The copolymerization kinetics were evaluated using quantitative *in situ* ^{13}C NMR kinetic measurements in bulk, demonstrating a higher reactivity of G over SSG monomer, leading to a gradient during the copolymerization process. Furthermore, we explored the redox-responsive degradation of the polymers upon treatment with a reducing agent, which resulted in selective degradation of the polymers into small segments. *In vitro* cytotoxicity studies, such as MTT and CCK-8 assays, revealed the superior biocompatibility of these novel polymers even at high concentrations (500 μg/mL). We anticipate that this new class of redox-labile polymer will contribute to the advancement and understanding of PG-based polymers and be a promising candidate for emerging materials and biomedical applications.

DOI: 10.1021/ma502242v
Macromolecules 2015, 48, 600−609

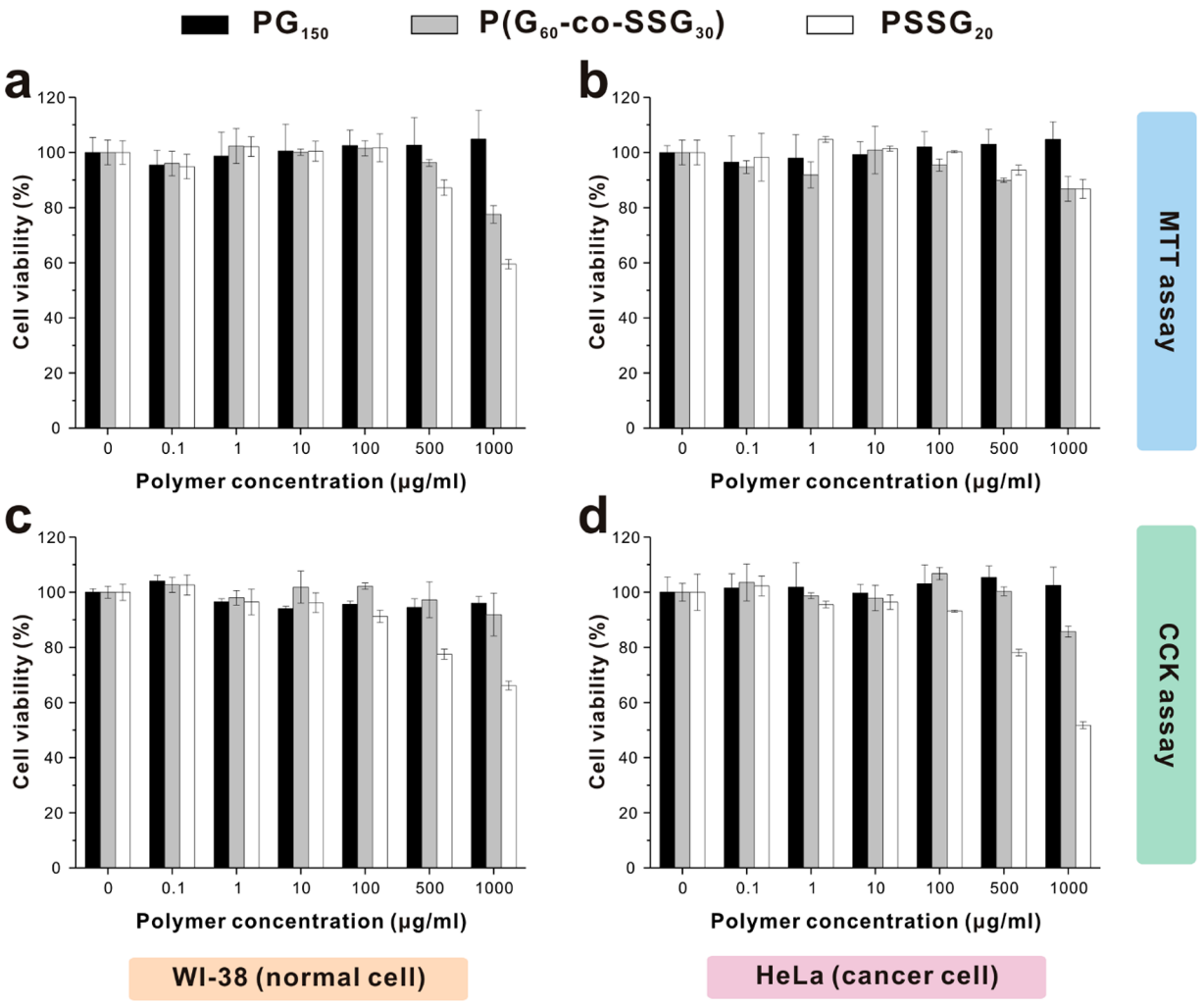

Figure 9. *In vitro* cell-viability assays of PG_{150} (black), $P(G_{60}$-*co*-$SSG_{30})$ (gray), and $PSSG_{20}$ (white) polymers determined by (a, b) MTT and (c, d) CCK assays using (a, c) WI-38 (normal cell) and (b, d) HeLa (cancer cell).

■ ASSOCIATED CONTENT

Supporting Information

Detailed ^{1}H and ^{13}C NMR spectra of SSG and PSSG, molecular weight calculation of PSSG homopolymer and P(G-*co*-SSG) copolymer, thermal stability of SSG monomer, additional description of the branched structure of PSSG, peak assignment of PSSG predicted by Mnova software, DSC graph for a simple blend of PG_{150} and $PSSG_{50}$, and GPC trace of PSSG and PG homopolymers before and after degradation. This material is available free of charge via the Internet at http://pubs.acs.org.

■ AUTHOR INFORMATION

Corresponding Author

*E-mail: bskim19@unist.ac.kr (B.-S.K.).

Notes

The authors declare no competing financial interest.

■ ACKNOWLEDGMENTS

This work was supported by the 2014 Research Fund (1.140101.01) of UNIST (Ulsan National Institute of Science & Technology). We thank Prof. Hyung-il Lee of University of Ulsan (Ulsan, Korea) for assistance with GPC measurement.

■ REFERENCES

(1) Wilms, D.; Stiriba, S.-E.; Frey, H. *Acc. Chem. Res.* **2009**, *43*, 129−141.
(2) Frey, H.; Haag, R. *Rev. Mol. Biotechnol.* **2002**, *90*, 257−267.
(3) Thomas, A.; Müller, S. S.; Frey, H. *Biomacromolecules* **2014**, *15*, 1935−1954.
(4) Sunder, A.; Hanselmann, R.; Frey, H.; Mülhaupt, R. *Macromolecules* **1999**, *32*, 4240−4246.
(5) Shenoi, R. A.; Brooks, D. E.; Kizhakkedathu, J. N. *J. Polym. Sci., Part A: Polym. Chem.* **2013**, *51*, 2614−2621.
(6) Kainthan, R. K.; Janzen, J.; Levin, E.; Devine, D. V.; Brooks, D. E. *Biomacromolecules* **2006**, *7*, 703−709.
(7) Lee, C. C.; MacKay, J. A.; Fréchet, J. M.; Szoka, F. C. *Nat. Biotechnol.* **2005**, *23*, 1517−1526.
(8) Nuhn, L.; Schüll, C.; Frey, H.; Zentel, R. *Macromolecules* **2013**, *46*, 2892−2904.
(9) Schüll, C.; Frey, H. *ACS Macro Lett.* **2012**, *1*, 461−464.
(10) Oikawa, Y.; Lee, S.; Kim, D. H.; Kang, D. H.; Kim, B.-S.; Saito, K.; Sasaki, S.; Oishi, Y.; Shibasaki, Y. *Biomacromolecules* **2013**, *14*, 2171−2178.
(11) Mangold, C.; Dingels, C.; Obermeier, B.; Frey, H.; Wurm, F. *Macromolecules* **2011**, *44*, 6326−6334.
(12) Obermeier, B.; Wurm, F.; Frey, H. *Macromolecules* **2010**, *43*, 2244−2251.
(13) Steinhilber, D.; Rossow, T.; Wedepohl, S.; Paulus, F.; Seiffert, S.; Haag, R. *Angew. Chem., Int. Ed.* **2013**, *52*, 13538−13543.

DOI: 10.1021/ma502242v
Macromolecules 2015, 48, 600−609

(14) Yang, S. K.; Shi, X.; Park, S.; Doganay, S.; Ha, T.; Zimmerman, S. C. *J. Am. Chem. Soc.* **2011**, *133*, 9964−9967.
(15) Imran ul-haq, M.; Hamilton, J. L.; Lai, B. F.; Shenoi, R. A.; Horte, S.; Constantinescu, I.; Leitch, H. A.; Kizhakkedathu, J. N. *ACS Nano* **2013**, *7*, 10704−10716.
(16) Lee, S.; Saito, K.; Lee, H.-R.; Lee, M. J.; Shibasaki, Y.; Oishi, Y.; Kim, B.-S. *Biomacromolecules* **2012**, *13*, 1190−1196.
(17) Son, S.; Shin, E.; Kim, B.-S. *Biomacromolecules* **2014**, *15*, 628−634.
(18) Calderón, M.; Graeser, R.; Kratz, F.; Haag, R. *Biorg. Med. Chem. Lett.* **2009**, *19*, 3725−3728.
(19) Kainthan, R. K.; Gnanamani, M.; Ganguli, M.; Ghosh, T.; Brooks, D. E.; Maiti, S.; Kizhakkedathu, J. N. *Biomaterials* **2006**, *27*, 5377−5390.
(20) Kleifeld, O.; Doucet, A.; auf dem Keller, U.; Prudova, A.; Schilling, O.; Kainthan, R. K.; Starr, A. E.; Foster, L. J.; Kizhakkedathu, J. N.; Overall, C. M. *Nat. Biotechnol.* **2010**, *28*, 281−288.
(21) Kainthan, R. K.; Janzen, J.; Kizhakkedathu, J. N.; Devine, D. V.; Brooks, D. E. *Biomaterials* **2008**, *29*, 1693−1704.
(22) Shenoi, R. A.; Lai, B. F.; Kizhakkedathu, J. N. *Biomacromolecules* **2012**, *13*, 3018−3030.
(23) Kainthan, R. K.; Brooks, D. E. *Biomaterials* **2007**, *28*, 4779−4787.
(24) Dingels, C.; Müller, S. S.; Steinbach, T.; Tonhauser, C.; Frey, H. *Biomacromolecules* **2013**, *14*, 448−459.
(25) Tonhauser, C.; Schüll, C.; Dingels, C.; Frey, H. *ACS Macro Lett.* **2012**, *1*, 1094−1097.
(26) Shenoi, R. A.; Lai, B. F.; Imran ul-haq, M.; Brooks, D. E.; Kizhakkedathu, J. N. *Biomaterials* **2013**, *34*, 6068−6081.
(27) Shenoi, R. A.; Narayanannair, J. K.; Hamilton, J. L.; Lai, B. F.; Horte, S.; Kainthan, R. K.; Varghese, J. P.; Rajeev, K. G.; Manoharan, M.; Kizhakkedathu, J. N. *J. Am. Chem. Soc.* **2012**, *134*, 14945−14957.
(28) Sun, H.; Meng, F.; Cheng, R.; Deng, C.; Zhong, Z. *Expert Opin. Drug Delivery* **2013**, *10*, 1109−1122.
(29) Chan, N.; An, S. Y.; Oh, J. K. *Polym. Chem.* **2014**, *5*, 1637−1649.
(30) Yan, Y.; Wang, Y.; Heath, J. K.; Nice, E. C.; Caruso, F. *Adv. Mater.* **2011**, *23*, 3916−3921.
(31) Jones, D. P.; Carlson, J. L.; Mody, V. C., Jr.; Cai, J.; Lynn, M. J.; Sternberg, P., Jr. *Free Radical Biol. Med.* **2000**, *28*, 625−635.
(32) Russo, A.; DeGraff, W.; Friedman, N.; Mitchell, J. B. *Cancer Res.* **1986**, *46*, 2845−2848.
(33) Saito, G.; Swanson, J. A.; Lee, K.-D. *Adv. Drug Delivery Rev.* **2003**, *55*, 199−215.
(34) Ko, N. R.; Oh, J. K. *Biomacromolecules* **2014**, *15*, 3180−3189.
(35) Chen, W.; Zou, Y.; Jia, J.; Meng, F.; Cheng, R.; Deng, C.; Feijen, J.; Zhong, Z. *Macromolecules* **2013**, *46*, 699−707.
(36) Lee, Y.; Koo, H.; Jin, G.-w.; Mo, H.; Cho, M. Y.; Park, J.-Y.; Choi, J. S.; Park, J. S. *Biomacromolecules* **2005**, *6*, 24−26.
(37) Wang, H.; Tang, L.; Tu, C.; Song, Z.; Yin, Q.; Yin, L.; Zhang, Z.; Cheng, J. *Biomacromolecules* **2013**, *14*, 3706−3712.
(38) Steinhilber, D.; Sisson, A. L.; Mangoldt, D.; Welker, P.; Licha, K.; Haag, R. *Adv. Funct. Mater.* **2010**, *20*, 4133−4138.
(39) Ryu, J.-H.; Chacko, R. T.; Jiwpanich, S.; Bickerton, S.; Babu, R. P.; Thayumanavan, S. *J. Am. Chem. Soc.* **2010**, *132*, 17227−17235.
(40) Mangold, C.; Wurm, F.; Obermeier, B.; Frey, H. *Macromolecules* **2010**, *43*, 8511−8518.
(41) Lee, B. F.; Wolffs, M.; Delaney, K. T.; Sprafke, J. K.; Leibfarth, F. A.; Hawker, C. J.; Lynd, N. A. *Macromolecules* **2012**, *45*, 3722−3731.
(42) Alkan, A.; Natalello, A.; Wagner, M.; Frey, H.; Wurm, F. R. *Macromolecules* **2014**, *47*, 2242−2249.
(43) Tominaga, H.; Ishiyama, M.; Ohseto, F.; Sasamoto, K.; Hamamoto, T.; Suzuki, K.; Watanabe, M. *Anal. Commun.* **1999**, *36*, 47−50.

DOI: 10.1021/ma502242v
Macromolecules 2015, 48, 600−609